Next Research 2 (2025) 100447

Contents lists available at ScienceDirect

Next Research

journal homepage: www.elsevier.com/locate/nexres

Comparative assessment of antibiofilm and antioxidant activities between *curcuma longa* silver nano particles and ethanolic extract of *curcuma longa*

Newton Suwal[a], Saroj Bashyal[a], Prem Paudyal[a], Dharma Prasad Khanal[a], Neelam Suwal[b], Saru Dhaubanjar[c], Rajan Thapa[d], Keshav Raj Paudel[e,f,*]

[a] Department of Pharmacy, Manmohan Institute of Health Sciences, Tribhuvan University, Kathmandu 44600, Nepal
[b] School of Public Health and Department of Community Medicine, Chitwan Medical College, Chitwan 44600, Nepal
[c] Department of Nursing, Nepal Medical College Pvt. Ltd., Kathmandu University, Kathmandu 44600, Nepal
[d] Department of Pharmacy, Universal college of medical sciences, Tribhuvan University, Bhairahawa, Rupendehi 32900, Nepal
[e] Centre for Inflammation, Centenary Institute and University of Technology Sydney, Faculty of Science, School of Life Sciences, Sydney 2007, Australia
[f] Uttaranchal Institute of Pharmaceutical Sciences, Uttaranchal University, Dehradun 248007, Uttarakhand, India

ARTICLE INFO

Keywords:
Curcuma longa
Silver-nanoparticles
Antioxidant
Antibiofilm
Staphylococcus aureus
Pseudomonas aeruginosa

ABSTRACT

Biofilms demonstrate multidrug resistance and present challenges for therapies. Notably, organisms like *Staphylococcus aureus* and *Pseudomonas aeruginosa* are major contributors to biofilm-related infections. Various strategies are employed to address antibiotic resistance vulnerabilities. Researchers are investigating the potential of plants and phytochemicals to overcome these challenges, with green nanosynthesis emerging as a promising strategy against antibiotic resistance. Turmeric (*Curcuma longa*) is a commonly used spice valued for its potent medicinal properties, such as antibacterial, anti-inflammatory, antioxidant, and anti-biofilm activities. This study encompasses the ethanolic extraction of *Curcuma longa* (*C. longaE*) and the qualitative identification of its constituents using Thin Layer Chromatography (TLC) and Gas Chromatography-Mass Spectrometry (GC–MS). Additionally, it also includes the synthesis and characterization of *Curcuma longa* silver nanoparticles (C. *longa*AgNPs), along with a comparative assessment of the antioxidant and antibiofilm activities of C. *longa*E and C. *longa*AgNPs. The TLC and GCMS– results show the presence of curcuminoids, Ar-tumerone, and curlone as major constituents in *C. longaE*. The *C. longaAgNPs* were characterized by Ultraviolet (UV) Spectroscopy, Fourier Transform Infrared Radiation (FTIR), X-ray Diffraction (XRD), and DLS analysis. The DLS analysis shows that *C. longaAgNPs* had a hydrodynamic diameter of 153 ± 0.75 nm and a polydispersity index (PDI) of 0.199 ± 0.0043. The IC_{50} value for the antioxidant activity of *C. longaAgNPs* was significantly lower at 19.972 ± 0.148 µg/ml when compared with the *C. longaE*, which measured 63.262 ± 0.928 µg/ml. The IC_{50} values for the antibiofilm activity of *C. longaAgNPs* were significantly lower at 0.1963 ± 0.0120 mg/ml for *P. aeruginosa* and 0.1681 ± 0.0259 mg/ml for *S. aureus* compared to the IC_{50} values of *C. longaE*, which measured 2.043 ± 0.0831 mg/ml and 0.8758 ± 0.0325 mg/ml, respectively. The *C. longaAgNPs* show significantly higher antioxidant and antibiofilm properties than *C. longaE*.

1. Introduction

Biofilms represent intricate communities of microorganisms enclosed within an extracellular matrix, which include proteins, extracellular DNA, lipids, and exopolysaccharides. These biofilms adhere to biological surfaces and are embedded within a hydrated matrix composed of extracellular polymeric substances (EPS) [1–4]. The EPS functions as an extra protective layer around the cells, forming a shield against diverse stresses. Consequently, bacteria within biofilms exhibit resistance to antibiotics and environmental pressures and can even evade the host immune response, posing significant challenges in clinical settings [5]. The emergence of multi-drug-resistant bacteria has led to investigation of novel strategies to combat microbial resistance. One such strategy involves targeting the quorum sensing (QS) mechanism as a potential alternative or complementary method to antibiotics. QS is chemical signaling process which is density-dependent mediated by acyl homoserine lactones (AHL). It regulates the expression of various genes involved in virulence determinants, bioluminescence, motility, plasmid transfer, enzyme and toxin secretion, bacteriocin production, efflux pump activity, and biofilm formation [4,6,7].

* Corresponding author at: Centre for Inflammation, Centenary Institute and University of Technology Sydney, Faculty of Science, School of Life Sciences, Sydney 2007, Australia, Uttaranchal Institute of Pharmaceutical Sciences, Uttaranchal University, Dehradun 248007, Uttarakhand, India.
E-mail address: Keshavraj.paudel@uts.edu.au (K.R. Paudel).

https://doi.org/10.1016/j.nexres.2025.100447
Received 18 March 2025; Received in revised form 15 May 2025; Accepted 21 May 2025

Medicinal plants abundant in secondary metabolites demonstrate strong antibacterial, antifungal, and antibiofilm activities [8]. These compounds can disrupt the QS system by inactivating receptors involved in QS signaling pathways. In the combat against biofilm resistance, additional approaches such as nanoparticles have been developed. Silver nanoparticles (AgNPs) exhibit antibiofilm activity by preventing bacterial cell adhesion to surfaces or disrupting intermolecular forces. AgNPs have also been shown to inhibit quorum sensing [9]. The synthesis of AgNPs using plant extracts offers several advantages in terms of safety, efficacy, cost, scalability, and production time [10,11]. The rhizome of *Curcuma longa (C. longa)* is a well-known culinary spice that showcases a range of medicinal attributes such as antibacterial, antimalarial, antiviral, antioxidant, antifungal, and anti-inflammatory properties [12]. Various research indicates that the ethanolic extract of *C. longa* contains elevated levels of polyphenols and flavonoids, leading to strong antioxidant effects. The biological effects are primarily due to its rich bioactive phytochemicals, with curcuminoids playing a crucial role [13]. Silver nanoparticles synthesized using plant extracts have garnered significant attention for their biological activities, including antioxidant, anticancer, and antimicrobial properties [14]. Results from earlier study indicate that the ethanolic extract of *C. longa* can effectively hinder biofilm formation produced by clinical isolates of *Pseudomonas aeruginosa* and *Staphylococcus aureus* [15]. The combination therapy utilizing AgNPs and *C. longa* is anticipated to enhance anti-biofilm activities [16] as well as antioxidant activity. In this study, our primary objective is to compare the antioxidant and antibiofilm activities between the ethanolic extract of *C. longa* (*C. longaE*) and *C. longa* silver nanoparticle (*C. longaAgNPs*). Subsequently, we aim to identify the phytochemicals present in the *C. longaE* using Thin Layer Chromatography (TLC) and Gas Chromatography and Mass Spectrometry (GC-MS), leveraging the benefits offered by these analytical techniques.

2. Materials and methods

2.1. Plants

C. longa rhizome were collected from the local market of Sindhuli district, located in Nepal at latitude 27°10′32.16″ North, longitude 85°56′30.84″ East. The collected rhizome was identified by the department of plant resources natural product research laboratory, Thapathali, Kathmandu, Nepal.

2.2. Extraction (C. longaE)

The rhizome of *C. longa* was cleaned with distilled water, followed by cutting it into small pieces and allowing it to dry in the shade for a month. Once completely dried, the rhizome was turned into a powder using an electric herbal grinding apparatus. Then, the Soxhlet extraction was performed by taking 20 g of this turmeric powder along with 250 ml of ethanol and resulting extracts were filtered through Whatsman filter paper #1. After filtration, the resulting filtrate was concentrated using a rotary evaporator (Rotavap) to remove the solvent under reduced pressure. Finally, the concentrated extract was preserved for further analysis by storing it at 4 °C, away from both light and moisture [15]. The curcuminoids in *C.longaE* were detected through TLC, while the essential oils in *C.longaE* were detected using GC-MS.

2.3. Silver nano-synthesis (C. longaAgNPs)

2.3.1. Extraction

The extraction process utilized water as a solvent. 20 g of powder were placed in a 250 ml beaker along with 100 ml of distilled water, then boiled for 20 min. After cooling, the decocted extract was filtered through Whatman filter paper #1 filter. The resulting filtrate *C. longa* aqueous extract (*C. longa* aq. extract) was employed for the synthesis of silver nanoparticles [17].

2.3.2. Preparation of silver nanoparticles (C. longaAgNPs)

To synthesize silver nanoparticles, 5 ml, 10 ml, 15 ml and 20 ml of the *C.longa* aq. extract were separately placed in 500 ml Conical Flasks. Subsequently, 90 ml of a 5 mM silver nitrate ($AgNO_3$) solution was added to each flask. The solutions were then stirred using a magnetic stirrer for 30 min. Color changes in the solutions were observed after 1 h, as well as after 24 and 48 h. The resulting colloidal suspensions of silver nanoparticles from *C. longa* aq. extract was centrifuged at 14,800 rpm for 15 min and washed five times to eliminate residual silver ions. The nanoparticles were subsequently dried under vacuum overnight at 25 °C, forming *C.longaAgNPs*. The synthesis involved using silver nitrate as the silver precursor and *C. longa* aq. extract as both a reductant and stabilizer for the nanoparticles [17].

2.3.3. Characterization of C. longaAgNPs

The characterization of *C.longaAgNPs* is done by using various instruments, including UV–visible spectroscopy, X-ray diffraction, FTIR, and DLS analysis.

UV–Visible Spectrophotometric Analysis

C. *longa*AgNPs were analyzed using UV–Visible Spectrophotometry (Shimadzu, Osaka, Japan) within a wavelength range of 200 to 800 nm. The distinct absorbance peak observed around 415–457 nm confirms the formation of silver nanoparticles, attributed to the surface plasmon resonance (SPR) of electrons on their surface. This technique provides valuable information regarding the nanoparticles' size, shape, stability, and concentration [18].

X-Ray Diffraction (XRD) Analysis

The crystalline structure and particle size of C. *longa*AgNPs were examined using an X-Ray Diffractometer (XRD-6000; Shimadzu). Measurements were carried out across a 2θ range of 0° to 80°, with a step size of 0.02° per min, under operating conditions of 30 kV and 10 mA. XRD analysis offers detailed insights into the nanoparticles' morphology and crystalline structure [19].

FTIR

FTIR spectral analysis was performed to determine the functional groups involved in the reduction of silver ions and the stabilization (capping) of bio-reduced AgNPs synthesized using *C. longa* aqueous extract. The spectra were recorded in the range of 400–4500 cm^{-1} using a PerkinElmer FT-IR Series 100, model 1650 spectrophotometer (Los Angeles, *CA*) [18].

Dynamic light scattering (DLS) analysis

Nanoparticle sizes were measured using a Zetasizer ZS Nano (Malvern Instruments, Malvern, UK), which utilizes a helium–neon (He–Ne) laser operating at a wavelength of 633 nm. All measurements were conducted at a controlled temperature of 25 °C. For particle size analysis, light scattering was recorded at a detection angle of 175° The dynamic light scattering (DLS) data, specifically the autocorrelation functions of the scattered light intensity, were processed using the manufacturer-supplied DTS 5.0 software. This analysis enabled the determination of hydrodynamic diameter distributions and the polydispersity index (PDI) calculation, which reflects the uniformity of particle size within the sample.

2.4. Antioxidant activity

The α, α-diphenyl-β-picrylhydrazyl (DPPH) free radical scavenging activity of different fractions were evaluated according to the method of Brand-Williamset et.al [20]. To prepare reference samples, we made solutions of ascorbic acid and sample solutions in ethanol at various concentrations (30, 25, 20, 15, 10, 5 μg/ml). A 0.1 mM DPPH solution was prepared in ethanol, and 4 ml of this solution was mixed with 1 ml of each sample at varying concentrations, along with ascorbic acid solutions. Then, the mixtures were allowed to stand for 30 min. As a negative control, we prepared a solution by mixing 4 ml of 0.1 mM DPPH with

1 ml of ethanol and kept it in the dark for 30 Min. Subsequently, we measured the absorbance at 517 nm. The ability to scavenge the DPPH radical was calculated using the following equation:

Scavenging percentage (%) = (Abs. Control- Abs. Test)/ Abs. Control*100

Where, Abs = absorbance.

2.5. *Antibiofilm activity comparison of* C. longaE *and* C. longaAgNPs

We used *S. aureus* and *P. aeruginosa* clinical isolates to examine *in vitro* biofilm formation assay which were obtained from Manmohan Memorial Medical College and Teaching Hospital, Kathmandu, Nepal. The *in vitro* biofilm formation assay, was performed as described by Suwal et al. [15]. The interpretation of biofilm production was based on criteria established by Stepanovic et al. [21] and the strong biofilm production strains were used for the evaluation of antibiofilm activity. The comparison of antibiofilm activity between *C. longaE* and *C. longaAgNPs* was conducted using 96-well microtiter plates with strong biofilm-producing *P. aeruginosa* and *S. aureus*. Fresh cultures of the test pathogens were mixed with 1 ml of fresh Luria-Bertani medium and exposed to different concentrations of *C. longaE* and *C. longaAgNPs* for 16 h at 30 ˚C without agitation for both test groups separately. After incubation, the free-floating cells were removed by washing the wells four times with sterile water. The cells adhered to the well surfaces were then stained with 0.2 percent crystal violet (CV) solution. Excess CV solution was removed after 10 min, and the CV-stained cells were solubilized using phosphate buffer and 95 percent glacial acetic acid. The quantitative analysis of biofilm was done by measuring optical density at 578 nm using a microtiter plate reader [15,22].

2.6. *Statistical analysis*

Each sample assessment was performed in triplicate. All results presented are means ± SEM of at least three independent experiments. GraphPad Prism 5.0 was used for statistical determination. Data were analyzed using an unpaired *t*-test, considering $p < 0.05$ as significant. The results shown are the mean ± SEM of at least three separate experiments.

3. Results

3.1. *Chemical identification of* C. longae

The presence of curcuminoids in *C. longaE*, specifically Curcumin, Bisdemethoxycurcumin (BDMC), and Demethoxycurcumin (DMC), was detected through TLC. During the separation of C. *longa*E on the TLC plate, each corresponding band produced a molecular ion peak consistent with those of the Curcumin, BDMC, and DMC standards as shown in Fig. 1, Table 1. The development process for each plate reached a height of about 5.8 cm, utilizing a mobile phase consisting of chloroform and methanol in a ratio of 19:1. Curcumin, BDMC, and DMC, were successfully identified in the *C. longaE* using TLC as shown in Fig. 1, Table 1. Additionally, the volatile components in *C. longaE* were identified using GCMS. A total of four peaks were recognized by comparison with a reference standard in the database, notably including a significant presence of ar-turmerone and curlone. The different constituents detected in *C. longaE* are tabulated below in Table 2, and the chromatogram is shown in Fig. 2.

Table 1
Detection of compounds in *C. longaE* by TLC.

TLC	Mobile Phase Ratio (Chloroform: Methanol)	RF Value		
		Curcumin	DMC	BDMC
Reference	19:1	0.75	0.55	0.39
Sample	19:1	0.731	0.548	0.27

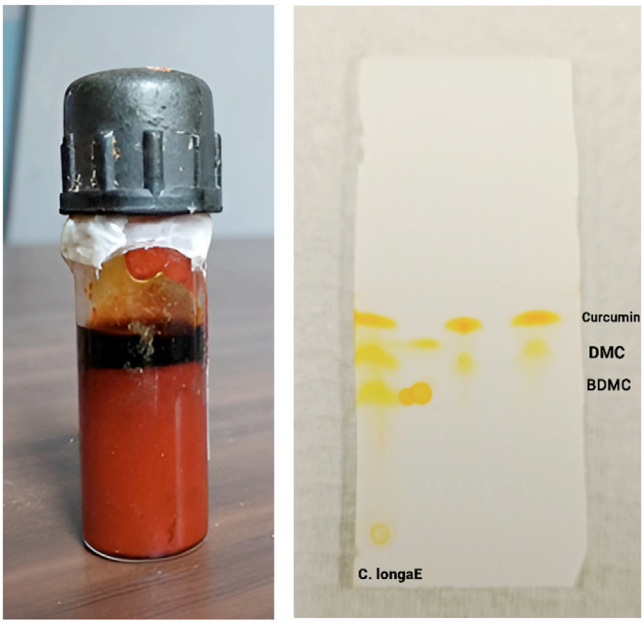

Fig. 1. *C. longaE* and TLC Profile (*C. longa* extract (*C.longaE*) was obtained through Soxhlet extraction and concentrated using a rotary evaporator (Rotavap). Thin-layer chromatography (TLC) was employed to detect the presence of curcuminoids in the extract.).

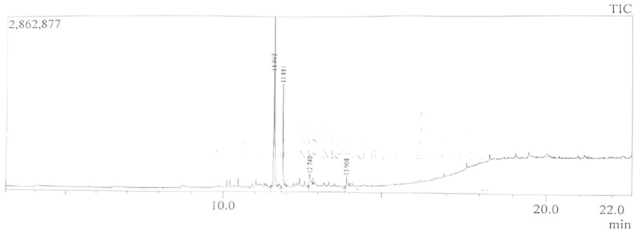

Peak Report TIC

Peak#	R.Time	Area	Area%	Height%	Name
1	11.592	6798586	67.23	47.89	Ar-tumerone
2	11.881	2383490	23.57	43.00	Curlone
3	12.740	582157	5.76	4.90	3-Buten-2-one, 4-(4-hydroxy-3-methoxyphenyl)-
4	13.908	348335	3.44	4.21	3-Decen-5-one
		10112568	100.00	100.00	

Fig. 2. GC–MS Chromatogram of *C. longaE.*

3.2. *Characterization of* C. longaAgNPs

3.2.1. *UV–visible spectroscopy analysis*

As the volume of *C. longa* extract increased, the intensity of the Surface Plasmon Resonance (SPR) peak also increased. This indicates the continuous reduction of silver ions and the corresponding increase in the concentration of silver nanoparticles (AgNPs). In particular, the SPR peak at 428 nm confirmed the formation of AgNPs when using a 5 mL *C. longa* aq. extract. Subsequently, as the volume of *C. longa* aq. extract increased to 10 mL, 15 mL, and 20 mL, the peak intensities at 427 nm, 427 nm, and 423 nm, respectively increased accordingly, as illustrated in Fig. 3. The nanoparticle synthesis process involved using silver nitrate as the silver precursor and *C. longa* aq. extract as both reductant and stabilizer for the nanoparticles. The UV-visible spectrum showed that the surface plasmon resonance (SPR) occurred in the range of 457–415 nm, indicating the presence of silver nanoparticles synthesized using *C. longa* aq. extract.

Table 2
Detection of compounds in *C. longaE* by GC–MS.

S.N.	Retention Time	Area	Area %	Height %	Name of Constituent
1	11.592	6798,586	67.23	47.89	Ar-tumerone
2	11.881	2383,490	23.57	43.00	Curlone
3	12.740	582,157	5.76	4.90	3-Buten-2-one, 4-(hydroxyl-3-methoxyphen
4	13.908	348,335	3.44	4.21	3-Decen-5-one

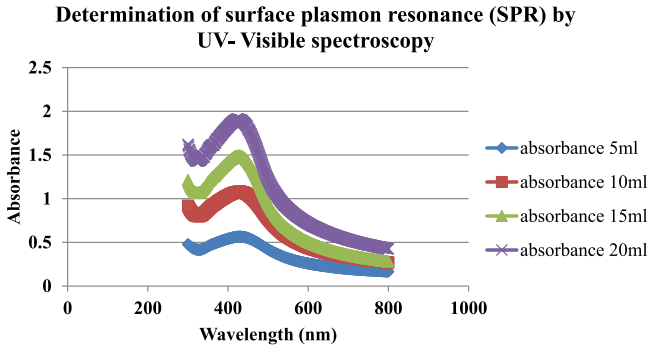

Fig. 3. Determination of surface plasmon resonance (SPR) by UV-visible spectroscopy.

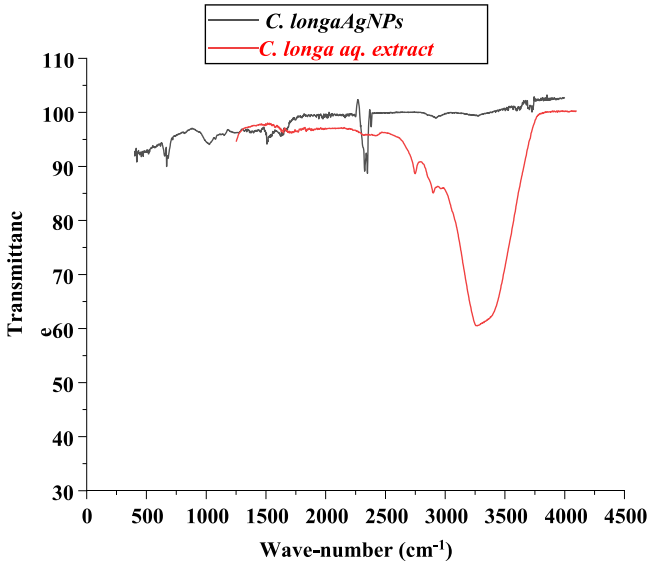

Fig.5. Fourier-transform infrared spectra for the *C.longa AgNPs* and *C. longa* aq. extract after 48 hrs biosynthesis reaction.

3.2.2. X-ray diffraction

The crystalline nature and size of nanoparticles are usually characterized using XRD. To characterize the crystalline nature and size of the *C. longaAgNPs*, we performed XRD analysis after 24 h of stirring. The XRD patterns of *C. longaAgNPs* demonstrated that the structure of the AgNPs formed was face-centered cubic. Moreover, all the *C. longaAgNPs* exhibited a similar diffraction pattern, with distinct peaks observed at 2θ angles of 38.18°, 44.25°, 64.72°, and 77.40° These peaks corresponded to the crystallographic planes of 111, 200, 220, and 311 respectively, within the face-centered cubic structure of silver crystals. The X-ray diffraction pattern is depicted in Fig. 4. Overall, the XRD pattern provided clear evidence that the *C. longaAgNPs* synthesized in this study possessed a crystalline nature.

Fourier transform infrared spectroscopy (FTIR)

The FTIR spectra analysis was conducted to identify the functional groups responsible for reducing silver-ions and the capping of bio-reduced AgNPs synthesized by the *C. longa aq. extract*. The transmission peaks observed in the *C. longaAgNPs* sample were recorded at 3323 cm^{-1}, 2902 cm^{-1}, 22,911.43 cm^{-1}, 942 cm^{-1}, 1627 cm^{-1}, 1637 cm^{-1}, 1417 cm^{-1}, 1147 cm^{-1}, 1004 cm^{-1}, 865 cm^{-1}, 692 cm^{-1}, and 510 cm^{-1} as depicted in Fig. 5.

Among these peaks, the absorption peaks around 865 cm^{-1}, 1004 cm^{-1}, and 1141 cm^{-1} can be attributed to the stretching vibrations of –C–N, –C–O–C, or –C–O groups respectively. These peaks suggest the presence of bonds derived from heterocyclic compounds such as alkaloids or flavones, as well as amide bonds, which are inherent in the *C.*

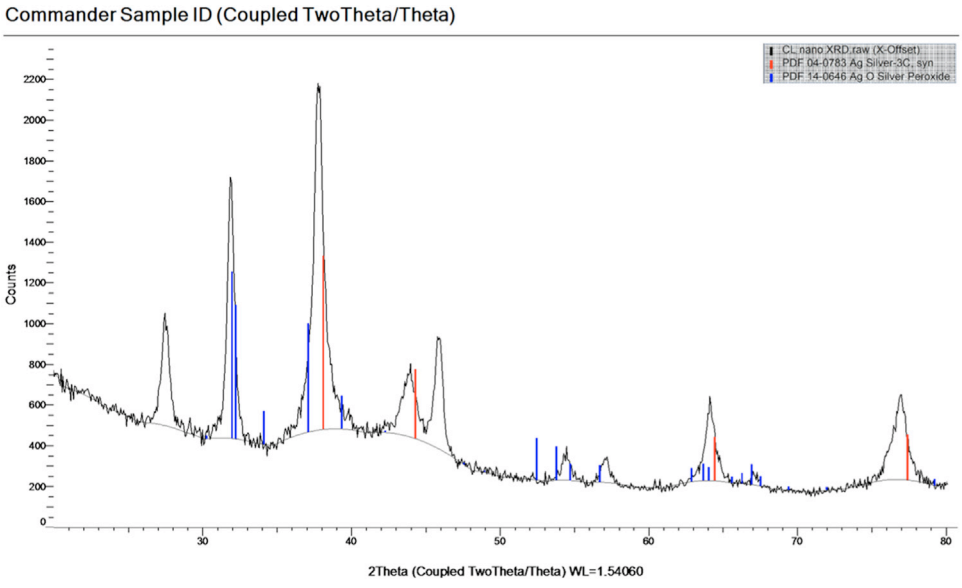

Fig.4. X-ray diffraction pattern of *C. longaAgNPs* after 24 hrs of stirring.

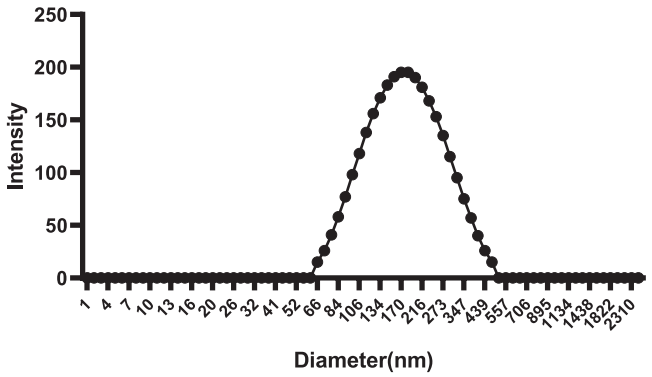

Fig. 6. DLS data of C. longaAgNPs with size distribution. Values are presented as Mean ± SEM (n = 3).

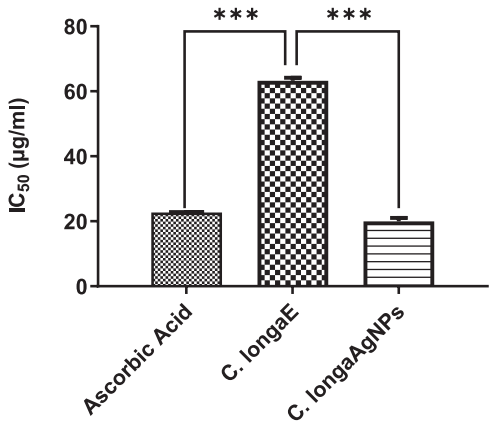

Fig. 7. Bar diagram of Antioxidant activity by *C. longaE* and *C. longaAgNPs*. Values are presented as Mean ± SEM (n = 3). $^{***}P < 0.001$ vs Ascorbic Acid, $^{\#\#\#}P < 0.001$ vs *C. longaE*.

longa. These bonds act as capping ligands for the nanoparticles, providing stabilization and functional properties to the AgNPs. Conversely, the absorption peak at 1627 cm^{-1} in the *C. longa* aq. extract, attributed to simultaneous $C = C$ and $C = O$ stretching, shifted to 1637 cm^{-1} in *C. longaAgNPs*. Additionally, the prominent absorption peak at 1147 cm^{-1}, associated with the enol C–O group in the *C. longa*aq. extract disappeared in *C. longaAgNPs*, likely due to the binding of silver (Ag) with the $C = O$ group in the *C. longa* aq. extract. There is also stretching around 2291.43 cm^{-1}, which is attributed to the presence of alkanes [23]. These alkanes may function as stabilizing or capping agents during the formation of nanoparticles, however, the role of these stretching bands in nanoparticle formation has not been reported in the literature. Additionally, the prominent absorption peak at 1147 cm^{-1}, associated with the enol C–O group in the *C. longa* aq. extract, disappeared in *C. longaAgNPs*, likely due to the binding of silver (Ag) with the $C = O$ group in the *C. longa* aq. extract. FTIR spectrum analysis reported the presence of different functional groups in turmeric powder responsible for capping *C. longaAgNPs*.

3.2.3. Dynamic light scattering (DLS)

The analysis showed that *C. longa*AgNPs had a hydrodynamic diameter of 153 ± 0.75 nm and a polydispersity index (PDI) of 0.199 ± 0.0043 as shown in Fig. 6. The measured size distribution and relatively low PDI indicate a narrow dispersion of particle sizes, suggesting a high degree of uniformity in the colloidal system. Such a low PDI value (<0.2) is typically indicative of mono dispersion, a desirable characteristic in nanoparticle formulations for biomedical applications, as it often correlates with improved stability, predictable biological interactions, and reproducibility in synthesis.

3.3. Antioxidant activity

The antioxidant capabilities of *C. longaE* and *C. longaAgNPs* were evaluated using the DPPH free radical scavenging assay. The IC_{50} for *C. longaAgNPs* was significantly lower at 19.972 ± 0.148 µg/ml compared to that of *C. longaE*, which was 63.262 ± 0.928 µg/ml. This indicates stronger antioxidant activity for the AgNPs. Compared with ascorbic acid, whose IC_{50} is 22.713 ± 1.047 µg/ml, the IC_{50} value of *C. longaAgNPs* is slightly lower, yet this difference is not statistically significant. This suggests that the antioxidant activity of *C. longaAgNPs* is like that of ascorbic acid. The results of this test are presented on Fig. 7.

3.4. Antibiofilm activity

Various strains of *P. aeruginosa* and *S. aureus*, specifically strong biofilm formation strains, were used in this comparative study. The efficacy of inhibiting biofilm formation by both *C. longaE* and *C. longaAgNPs* in these bacterial strains was found to be contingent on the concentration applied. The IC_{50} values for *C. longaAgNPs* were significantly lower at 0.1963 ± 0.0120 mg/ml for *P. aeruginosa* and 0.1681 ± 0.0259 mg/ml for *S. aureus* compared to the IC_{50} values of *C. longaE*, which measured 2.043 ± 0.0831 mg/ml and 0.8758 ± 0.0325 mg/ml, respectively. The result of antibiofilm activity is shown in Table 3 and Fig. 8.

4. Discussion

Chronic infections often result in antimicrobial treatment failure with antibiotics due to the transition of bacteria from free-swimming forms to structured biofilms, which are significantly more resistant (up to 1000 times) than planktonic bacteria [24]. Biofilms impede antibiotic penetration through their extracellular matrix by restricting diffusion or neutralizing antimicrobial agents with polysaccharides [25]. Silver nanoparticles have demonstrated improved uptake and availability at infection sites, attaching directly to cell membranes or penetrating cell walls more effectively than silver ions [26]. We identified the presence of Curcumin, BDMC, and DMC using TLC in *C. longaE* and these curcuminoids demonstrate various biological effects acting as antioxidants, antibiofilm, neuroprotective agents, antitumor substances, anti-inflammatory compounds, anti-acidogenic agents, radioprotective agents, and contributors to arthritis management [27,28]. The GC–MS

Table 3
% of biofilm inhibition by *C. longaE and C. longaAgNPs*.

Conc. (mg/ml)	Biofilm Inhibition by *C. longaE (%)*						Biofilm Inhibition by *C. longaAgNPs (%)*					
	P. aeruginosa			*S. aureus*			*P. aeruginosa*			*S. aureus*		
	P_9	P_{10}	P_4	S_{156}	S_{224}	S_{29}	P_9	P_{10}	P_4	S_{156}	S_{224}	S_{29}
0.2	15.206	14.027	12.870	26.116	24.863	29.176	44.587	45.928	42.086	46.652	47.541	48.235
0.4	23.454	20.814	21.478	39.509	34.153	38.588	64.691	60.633	69.739	60.714	68.306	64.235
0.8	27.577	24.434	25.913	47.545	45.082	44.000	73.196	75.339	77.826	71.875	77.322	75.529
1	30.670	29.864	31.652	57.143	54.372	53.647	76.546	77.602	78.348	78.348	83.060	84.000

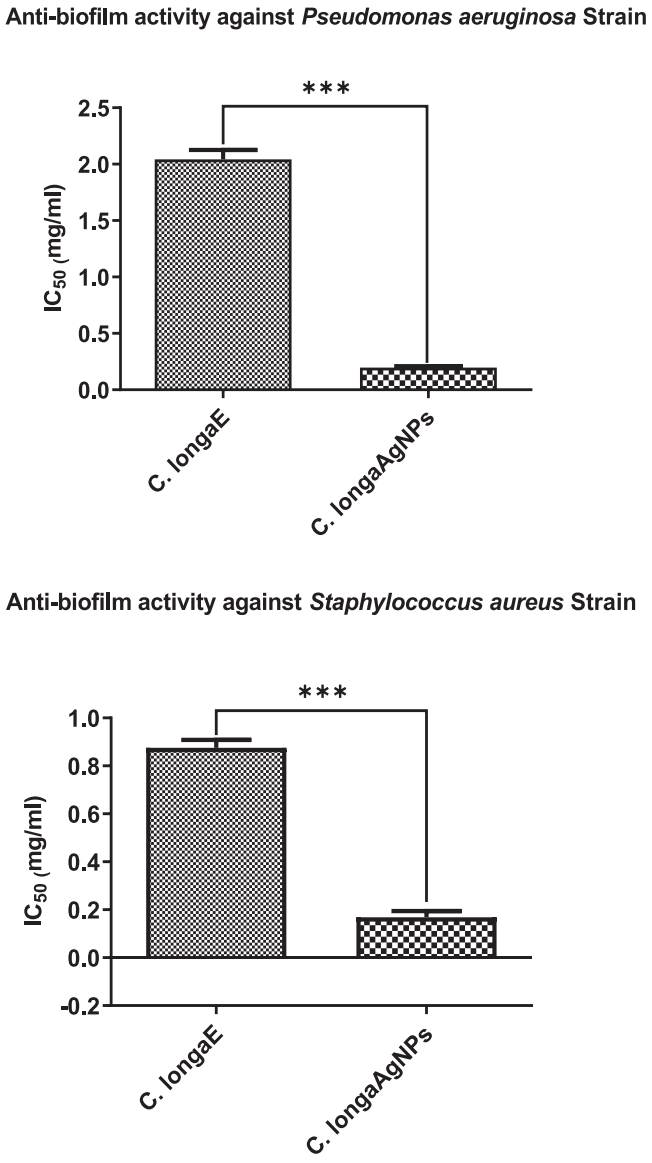

Fig. 8. Bar diagram of IC_{50} Value of *C. longaE and C. longaAgNPs*. Values are presented as Mean ± SEM ($n = 3$). P value is calculated by using *t*-test. $^{***}P < 0.001$ *C. longaE vs C.longaAgNPs.*

results show the presence of Ar-tumerone and curlone as major constituents in *C. longaE* that demonstrate a range of bioactivities, including antioxidant, antibacterial, antifungal, antiparasitic, anti-inflammatory, antidiabetic, anticancer, analgesic, nephroprotective, and insecticidal properties [29].

The *C. longaAgNPs* were characterized by UV-visible Spectroscopy, FTIR, XRD, and DLS. The UV spectrum showed that the surface plasmon resonance (SPR) occurred in the range of 457–415 nm, indicated the presence of silver nanoparticles which is similar as finding attained by Shameli et al. 2014 [17], where the presence of surface plasmon absorption maxima was observed at different wavelengths: 457 nm, 455 nm, 450 nm, and 417 nm for 1 mL, 2 mL, 5 mL, and 10 mL of turmeric extract, respectively. In green nano synthesis, XRD is one of the most versatile and non-destructive techniques widely used for characterizing the crystal structure, orientation, size, size, crystallinity, and defects of nanoparticles. The information obtained from the XRD peaks is crucial for determining whether the synthesized nanoparticles are amorphous or crystalline in nature [30,31]. The XRD patterns of *C. longaAgNPs* demonstrated that the structure of the AgNPs formed was face-centered cubic. Our observations were confirmed by a similar study by Shameli, Ahmad et al. (2014) [17] supporting the reliability and consistency of the synthesis and measurement techniques used in this study. This small particle size increases the effective surface area, which helps improve antibiofilm and antimicrobial activity. The FTIR spectra analysis was conducted to identify the functional groups responsible for reducing Ag ions and the capping of bio-reduced AgNPs synthesized by the *C. longa aq.* extract. FTIR peaks suggest the presence of bonds derived from heterocyclic compounds such as alkaloids or flavones, as well as amide (I) bonds, and these bonds act as capping ligands for the nanoparticles, providing stabilization and functional properties to the AgNPs. Similar findings were also found by yang et.al (2016) [32]. Dynamic light scattering (DLS) analysis demonstrated that the silver nanoparticles (C. *longa*AgNPs) possessed an average hydrodynamic diameter of 153 ± 0.75 nm and a polydispersity index (PDI) of 0.199 ± 0.0043. These particle size and dispersion measurements further suggest that nanoparticle formation followed a sequential mechanism, likely beginning with nucleation and followed by regulated growth and minimal aggregation. The findings are consistent with the report by Sathishkumar et al. [33] and Shameli et al. (2012) [18], who observed comparable nanoparticle formation dynamics and size profiles in their study on biologically synthesized silver nanoparticles. In our study, the synthesized nanoparticles were characterized using UV–Visible spectroscopy, Fourier Transform Infrared Spectroscopy (FTIR), X-ray Diffraction (XRD) analysis, and Dynamic Light Scattering (DLS) analysis. These techniques provided crucial insights into the optical properties, functional groups, crystalline nature, and size of the nanoparticles. Although Scanning Electron Microscopy (SEM) and Transmission Electron Microscopy (TEM) are powerful tools for confirming particle size, shape, and surface morphology, we were unfortunately unable to perform these analyses due to limitations in funding and facility access. As a result, the characterization of *Curcuma longa*-mediated silver nanoparticles (*C. longa*-AgNPs) was confined to UV, FTIR, XRD and DLS techniques. Despite this limitation, the results obtained from the employed methods sufficiently support the successful synthesis of the nanoparticles.

C. longaAgNPs demonstrate significantly higher antioxidant activity than *C. longaE.* The antioxidant effectiveness of *C. longaAgNPs* is akin to that of ascorbic acid. The antioxidant property of *C. longaE* exhibited higher antioxidant properties than other drugs in different studies [34,35]. This similarity is attributed to the presence of phenolic and chemical components of the *C. longa.* In TLC and GCMS analysis, we detected the curcuminoids, Ar-turmerone and curlone, which have been suggested to show antioxidant properties. The antioxidant effectiveness of *C. longaAgNPs* surpasses that of *C. longaE*, likely attributable to the presence of phenolic and chemical constituents on the surface of the silver nanoparticles. The findings are consistent with the research conducted by D. Arumai, et al., which indicated that the silver nanoparticles derived from turmeric extract exhibit superior antioxidant properties compared to ascorbic acid [36].

These findings of the antibiofilm study underscore the considerable superiority of *C. longaAgNPs* in hindering biofilm formation compared to *C. longaE*. These findings are consistent with a prior study by Nurjamil, Aris Muhamad, et al. [37], which reported that the IC_{50} value of silver nanoparticles from *Curcuma heyneana* rhizome needed to inhibit biofilm formation was 29.29 μg/ml in *P. aeruginosa* and 26.21 μg/ml in *S. aureus*. Biofilms possess high levels of resistance to traditional antibiotics, exhibiting up to a 1000-fold increase in resistance. This resistance is primarily attributed to the EPS matrix, which hinders the penetration of antibiotics by restricting diffusion or neutralizing antimicrobial agents through interaction with the extracellular polysaccharides [38]. The capability of *C. longaE* and *C. longaAgNPs* to prevent biofilm formation in these bacteria was determined to be dependent on the concentrations used. These results highlight the significant effectiveness of *C. longaAgNPs* over *C. longaE* in inhibiting biofilm formation. Experimental outcomes showed that silver nanoparticles from *C. longa* were effective in antibiofilm activity, diminishing the bacteria capacity to adhere to

a polystyrene surface. This was indicated by a decrease in absorbance compared to untreated cells. Ching-Yee Loo et al., also found that the combination of curcumin and silver nanoparticles exhibited synergistic antibiofilm effects, reducing the formation and viability of biofilms [39]. Curcumin interferes with quorum-sensing systems that regulate bacterial virulence factors, likely due to the β-diketone moiety in its chemical structure, which allows it to form complexes with metal ions [40]. The reduction of QS-dependent factors like exopolysaccharide, alginate, and motility behaviors (including swimming and swarming) by curcumin indirectly verifies that curcumin antibiofilm actions are primarily through inhibiting the biofilm formation process, rather than by directly killing bacteria [41]. It was supposed to be the combined effect of curcuminoids and other chemical components in the *C. longaAgNPs*, effectively inhibiting biofilm formation. The phytochemicals in *C. longa*, such as curcumin, demethoxycurcumin, bisdemethoxycurcumin, and other phenolic compounds, possess intrinsic antioxidant and antimicrobial properties. When these compounds are utilized in the green synthesis of AgNPs, they not only act as reducing and stabilizing agents but also become integrated or adsorbed on the nanoparticle surface. This integration can lead to a higher local concentration of bioactive molecules, enhanced surface reactivity, and improved stability, thereby increasing the overall bioactivity of the nanoparticles compared to the crude plant extract alone. In terms of antioxidant activity, the nanoscale size of the particles results in a larger surface area, facilitating greater interaction with free radicals. For antibiofilm activity, AgNPs are known to disrupt bacterial membranes, interfere with quorum sensing, and inhibit biofilm matrix formation mechanisms that are further enhanced by the bioactive compounds from *C. longa*. Several studies have reported similar observations. For example, Singh et al. (2018) and Ahmed et al. (2016) demonstrated that C. *longa*-AgNPs exhibited significantly higher antimicrobial and antioxidant activity than the *C. longa* extract alone, attributing this to the synergistic effects and enhanced cellular uptake due to the nanoformulation [42,43]. In the present study, we aimed to assess the enhanced bioactivity, specifically antioxidant and antibiofilm potential, of *C. longa*AgNPs, in comparison to the extract alone *C. longa*E. Although it is well-established that silver nanoparticles (AgNPs) exhibit intrinsic bioactivities, an AgNP-only control was not included due to methodological constraints and to maintain consistency with the green synthesis approach. This approach, wherein *C. longa* extract acts as both the reducing and capping agent, inherently integrates the bioactive constituents of the plant into the nanoparticle surface, making it scientifically inconsistent to compare with chemically synthesized AgNPs, which would differ significantly in particle size, surface chemistry, and biological behavior. This approach is consistent with several studies in the literature that have evaluated plant-extract-mediated AgNPs without incorporating chemically synthesized AgNP controls. For example, Rajivgandhi et al. (2020) demonstrated that AgNPs synthesized from *Gracilaria corticata* showed strong antioxidant and antibiofilm activity against *Klebsiella pneumoniae*, without comparing them to AgNPs alone [44]. Similarly, Mohanta et al. (2020) reported potent antibacterial and antibiofilm effects of AgNPs biosynthesized from various Indian medicinal plants, again omitting an AgNP-only group [45]. Ikram et al. (2021) also observed enhanced antibiofilm activity of AgNPs synthesized using *Narcissus tazetta* extract against *Escherichia coli* and *S. aureus*, focusing on the synergistic impact of phytochemicals and silver [46]. These examples reflect a common practice in green nanotechnology research, where the primary aim is to assess the improvement in bioactivity due to phytochemical-silver synergy rather than isolating the effect of silver alone. Nonetheless, we recognize that including a chemically synthesized AgNP control in future work would offer a more detailed understanding of the individual contributions of silver and plant compounds.

Our results indicate that *C. longaAgNPs* exhibit superior antioxidant and antibiofilm activity compared to *C. longaE*, and they have the potential to serve as therapeutic agents in combating antibiotic resistance caused by biofilm producing bacteria.

5. Conclusions

In this study, we examined and contrasted the antioxidant and antibiofilm properties of *C. longaE* and *C. longaAgNPs*. Our results showed that, *C. longaAgNPs* produce more potent antioxidant and antibiofilm activities compared to *C. longaE.* Additionally, there was a significant difference between inhibitory effects on novel biofilm formation between *C. longaE* and *C. longaAgNPs.* Both the *C. longaE* and *C. longaAgNPs* proved effective in terms of antioxidant activity and tackling biofilms by diminishing their formation and persistence. Nonetheless, it is important to emphasize the need for further studies to understand the loading efficiency of turmeric extract, its effectiveness *in vivo*, safety, and potential utilizations.

Abbreviations

C.longa: Curcuma Longa, C.longaE: Ethanolic extract of *Curcuma longa, C. longaAgNPs: Curcuma longa* silver nano particle, *S. aureus: Staphylococcus aureus, P. aeruginosa: Pseudomonas aeruginosa*, EPS: Extracellular polymeric substance, SPR: Surface plasmon resonance, CV: Crystal Violet, XRD: X-ray diffraction, FTIR: Fourier transforms infrared spectroscopy, $AgNO_3$: silver nitrate.

Availability of data and materials

The datasets utilized and/or examined during the present study can be obtained from the corresponding author upon reasonable request.

Ethics approval and consent to participate

Not applicable.

Consent for publication

Not applicable.

Funding statement

This study was carried out without the support of external funding.

Competing interests

The authors declare that they have no competing interests.

Declaration of competing interest

The authors declare that they have no known competing financial interests or personal relationships that could have appeared to influence the work reported in this paper.

CRediT authorship contribution statement

Newton Suwal: Writing – original draft, Validation, Software, Methodology, Investigation, Formal analysis, Data curation, Conceptualization. **Saroj Bashyal:** Writing – original draft, Data curation, Conceptualization. **Prem Paudyal:** Writing – review & editing, Supervision. **Dharma Prasad Khanal:** Writing – review & editing, Supervision. **Neelam Suwal:** Writing – review & editing. **Saru Dhaubanjar:** Writing – review & editing. **Rajan Thapa:** Writing – review & editing, Formal analysis. **Keshav Raj Paudel:** Writing – review & editing, Supervision, Conceptualization.

References

[1] H.-C. Flemming, J. Wingender, The biofilm matrix, Nat. Rev. Microbiol. 8 (9) (2010) 623–633.
[2] Y. Irie, et al., Pseudomonas aeruginosa biofilm matrix polysaccharide psl is regulated transcriptionally by RpoS and post-transcriptionally by RsmA, Mol. Microbiol. 78 (1) (2010) 158–172.

[3] A.D. Verderosa, M. Totsika, K.E. Fairfull-Smith, Bacterial biofilm eradication agents: a current review, Front. Chem. 7 (2019) 495483.
[4] K. Alam, et al., Anti-biofilm activity of plant derived extracts against infectious pathogen-Pseudomonas aeruginosa PAO1, J. Infect. Public. Health. 13 (11) (2020) 1734–1741.
[5] H.-S. Kim, H.-D. Park, Ginger extract inhibits biofilm formation by Pseudomonas aeruginosa PA14, PloS One 8 (9) (2013) e76106.
[6] T.R. De Kievit, B.H. Iglewski, Bacterial quorum sensing in pathogenic relationships, Infect. Immun. 68 (9) (2000) 4839–4849.
[7] H. Hirakawa, H. Tomita, Interference of bacterial cell-to-cell communication: a new concept of antimicrobial chemotherapy breaks antibiotic resistance, Front Microbiol 4 (2013) 114.
[8] F.A. de Almeida, et al., Virtual screening of plant compounds and nonsteroidal anti-inflammatory drugs for inhibition of quorum sensing and biofilm formation in Salmonella, Microb. Pathog. 121 (2018) 369–388.
[9] K. Kalishwaralal, et al., Silver nanoparticles impede the biofilm formation by Pseudomonas aeruginosa and Staphylococcus epidermidis, Colloids Surfaces B 79 (2) (2010) 340–344.
[10] M.G. Aboelmaati, et al., Biogenic and biocompatible silver nanoparticles for an apoptotic anti-ovarian activity and as polydopamine-functionalized antibiotic carrier for an augmented antibiofilm activity, Colloids Surfaces B. 206 (2021) 111935.
[11] N.S. Swidan, et al., Antibiofilm activity of green synthesized silver nanoparticles against biofilm associated enterococcal urinary pathogens, Sci. Rep. 12 (1) (2022) 3869.
[12] S. Abdel-Shafy, et al., Efficacy and safety of ethanolic Curcuma longa extract as a treatment for sand tampan ticks in a rabbit model, Vet. World. 13 (4) (2020) 812.
[13] M. Grover, et al., In vitro phytochemical screening, cytotoxicity studies of Curcuma longa extracts with isolation and characterisation of their isolated compounds, Molecules 26 (24) (2021) 7509.
[14] M. Khatun, et al., Green synthesis of silver nanoparticles using extracts of Mikania cordata leaves and evaluation of their antioxidant, antimicrobial and cytotoxic properties, Food Chem. Adv. 3 (2023) 100386.
[15] N. Suwal, et al., Antimicrobial and antibiofilm potential of Curcuma longa Linn. Rhizome extract against biofilm producing Staphylococcus aureus and Pseudomonas aeruginosa isolates, Cell. Mol. Biol. 67 (1) (2021) 17–23.
[16] P.R. Arya, et al., Antioxidant, antibacterial and antibiofilm potential of green synthesized silver-zinc oxide nanocomposites from Curcuma longa extract against multi-drug-resistant enteroaggregative E. coli, Medical Sciences Forum, MDPI, 2023.
[17] K. Shameli, et al., Effect of Curcuma longa tuber powder extract on size of silver nanoparticles prepared by green method, Res. Chem. Intermed. 40 (2014) 1313–1325.
[18] K. Shameli, et al., Green biosynthesis of silver nanoparticles using Curcuma longa tuber powder, Int. J. Nanomed. 7 (2012) 5603–5610.
[19] K. Rajak, et al., Green Synthe. Silver Nanoparticles Using Curcuma Longa Flower Extract, Antibacteri. Activ (2023).
[20] W. Brand-Williams, M.-E. Cuvelier, C. Berset, Use of a free radical method to evaluate antioxidant activity, LWT-Food Sci. Technol. 28 (1) (1995) 25–30.
[21] G.D. Christensen, et al., Adherence of coagulase-negative staphylococci to plastic tissue culture plates: a quantitative model for the adherence of staphylococci to medical devices, J. Clin. Microbiol. 22 (6) (1985) 996–1006.
[22] I.A.S.V. Packiavathy, et al., Antibiofilm and quorum sensing inhibitory potential of cuminum cyminum and its secondary metabolite methyl eugenol against gram negative bacterial pathogens, Food Res. Int. 45 (1) (2012) 85–92.
[23] M. Maghimaa, S.A. Alharbi, Green synthesis of silver nanoparticles from Curcuma longa L. and coating on the cotton fabrics for antimicrobial applications and wound healing activity, J. Photochem. Photobiol. B 204 (2020) 111806.
[24] H. Ishida, et al., In vitro and in vivo activities of levofloxacin against biofilm-producing Pseudomonas aeruginosa, Antimicrob. Agents Chemother. 42 (7) (1998) 1641–1645.
[25] J.G. Elkins, et al., Protective role of catalase in Pseudomonas aeruginosa biofilm resistance to hydrogen peroxide, Appl. Environ. Microbiol. 65 (10) (1999) 4594–4600.
[26] I. Sondi, B. Salopek-Sondi, Silver nanoparticles as antimicrobial agent: a case study on E. coli as a model for gram-negative bacteria, J. Colloid Interface. Sci. 275 (1) (2004) 177–182.
[27] A. Amalraj, et al., Biological activities of curcuminoids, other biomolecules from turmeric and their derivatives–A review, J. Tradit. Complement. Med. 7 (2) (2017) 205–233.
[28] M. Karaman, F. Fırıncı, I. Bahar, Effects of imipenem, tobramycin and curcumin on biofilm formation of Pseudomonas aeruginosa strains, Mikrobiyol. Bul. 47 (1) (2013) 192–194.
[29] A.M. Orellana-Paucar, M.G. Machado-Orellana, Pharmacological profile, bioactivities, and safety of turmeric oil, Molecules 27 (16) (2022) 5055.
[30] M. Ghasempour-Mouziraji, et al., A review study on metal powder materials and processing parameters in Laser Metaleposition, Optics. Laser Technol. 170 (2024) 110226.
[31] M. Majithia, D.A. Barretto, Biocompatible green-synthesized nanomaterials for therapeutic applications, in: Advances in Nano and Biochemistry, Elsevier, 2023, pp. 285–367.
[32] X.X. Yang, C.M. Li, C.Z. Huang, Curcumin modified silver nanoparticles for highly efficient inhibition of respiratory syncytial virus infection, Nanoscale 8 (5) (2016) 3040–3048.
[33] M. Sathishkumar, K. Sneha, Y.S. Yun, Immobilization of silver nanoparticles synthesized using Curcuma longa tuber powder and extract on cotton cloth for bactericidal activity, Bioresour. Technol. 101 (20) (2010) 7958–7965.
[34] S.W. Qader, et al., Antioxidant, total phenolic content and cytotoxicity evaluation of selected Malaysian plants, Molecules 16 (4) (2011) 3433–3443.
[35] E. Tanvir, et al., Antioxidant properties of popular turmeric (Curcuma longa) varieties from Bangladesh, J. Food Qual. 2017 (2017).
[36] D.A. Selvan, et al., Garlic, green tea and turmeric extracts-mediated green synthesis of silver nanoparticles: phytochemical, antioxidant and in vitro cytotoxicity studies, J. Photochem. Photobiol. B. 180 (2018) 243–252.
[37] A.M. Nurjamil, et al., Effectivity of silver nanoparticles-temu giring (Curcuma heyneana) rhizome on inhibiting the growth of bacteria causing nosocomial infection, HAYATI J. Biosci. 31 (2) (2024) 284–292.
[38] F. Reffuveille, et al., A broad-spectrum antibiofilm peptide enhances antibiotic action against bacterial biofilms, Antimicrob. Agents Chemother. 58 (9) (2014) 5363–5371.
[39] C.-Y. Loo, et al., Combination of silver nanoparticles and curcumin nanoparticles for enhanced anti-biofilm activities, J. Agric. Food Chem. 64 (12) (2016) 2513–2522.
[40] T. Rudrappa, H.P. Bais, Curcumin, a known phenolic from Curcuma longa, attenuates the virulence of Pseudomonas aeruginosa PAO1 in whole plant and animal pathogenicity models, J. Agric. Food Chem. 56 (6) (2008) 1955–1962.
[41] I.A.S.V. Packiavathy, et al., Inhibition of biofilm development of uropathogens by curcumin–an anti-quorum sensing agent from Curcuma longa, Food Chem 148 (2014) 453–460.
[42] M.S. Tawre, et al., Synergistic and antibiofilm potential of Curcuma aromatica derived silver nanoparticles in combination with antibiotics against multidrug-resistant pathogens, Front Chem. 10 (2022) 1029056.
[43] A. Pramana, et al., Reduction of biofilm and pathogenic microorganisms using curcumin-mediated photodynamic inactivation to prolong food shelf-life, Int. J. Food Microbiol. 425 (2024) 110866.
[44] G.N. Rajivgandhi, et al., Anti-oxidant, anti-bacterial and anti-biofilm activity of biosynthesized silver nanoparticles using Gracilaria corticata against biofilm producing K. pneumoniae, Colloids Surfaces A. 600 (2020) 124830.
[45] Y.K. Mohanta, et al., Anti-biofilm and antibacterial activities of silver nanoparticles synthesized by the reducing activity of phytoconstituents present in the Indian medicinal plants, Front Microbiol. 11 (2020) 1143.
[46] P. Negi, et al., Antimicrobial and antibiofilm potential of green-synthesized graphene-silver nanocomposite against multidrug-resistant nosocomial pathogens, Biomedicines 12 (5) (2024).